Supplementary information

Role of structure and electron mobilization in enhanced ethanol sensing by Al doped SnO_2 nanoparticles

*Nirman Chakraborty,[1] Sagnik Das,[1] Velaga Srihari,[2] Dibya Jyoti Mondal,[3] Debdulal Saha,[1] Sanjit Konar,[3] Ajay K. Mishra[2] and Swastik Mondal[1]**

[1]CSIR Central Glass and Ceramic Research Institute, 196, Raja S. C. Mullick Road, Jadavpur, Kolkata 700032, India

[2]High Pressure & Synchrotron Radiation Physics Division, Bhabha Atomic Research Centre, Trombay, Mumbai-400085, India

[3]Department of Chemistry, Indian Institute of Science Education and Research (IISER) Bhopal, Bhauri, Bhopal 462066, India

[*]Corresponding author: swastik_mondal@cgcri.res.in

Synthesis

The calcination temperature was determined by mass loss studies using Thermo Gravimetric Analysis (TGA) in a NETZSCH STA 449 C TGA analyser from room temperature to 1000°C at the rate of 5°C/min (Fig. S2). An empty Al_2O_3 crucible was used as reference.

XRD data collection scheme

Synchrotron based room temperature powder X-ray diffraction measurements were carried out on well ground powder samples at Extreme Conditions Angle Dispersive/Energy dispersive X-ray diffraction (EC-AD/ED-XRD) beamline (BL-11) at Indus-2 synchrotron source, Raja Ramanna Centre for advanced Technology (RRCAT), Indore, India. Desired wavelength for ADXRD diffraction experiments was selected from the white light from the bending magnet using a Si (111) channel cut monochromator. The monochromatic beam was then focused on to the sample with a Kirkpatrick-Baez mirror. A MAR345 image plate area detector was used to collect 2 dimensional diffraction data. Sample to detector and the wavelength of the beam were calibrated using NIST standards LaB_6 and CeO_2. Calibration and conversion/integration of 2D diffraction data to 1D intensity vs. 2theta was carried out using FIT2D software.

Sample preparation for UV-Vis studies

For UV-Vis spectroscopic measurements, small amounts of sample were uniformly dispersed in iso-propyl alcohol using a probe sonicator (Hilscher) for 30 minutes followed by uniformity checking with Tyndall effect experiment. Quartz cuvettes with 10 mm path length and a top Teflon cover were filled with the samples and data were recorded from 200 nm to 800 nm with scan rate of 10 nm/sec. Background corrections were done with pure solvents. For the 50°C data, the dispersed solution was placed on a flat heater at 50°C and temperature was recorded by an IR gun repeatedly. The cuvettes were immediately filled with the heated liquid and data was recorded. Similar approach was adopted for the 70°C case also. Since it is a comparative study performed under identical conditions, the errors that have crept in due to crudeness of the experiment were equally present among all data and hence their effect was nullified once comparisons were done. Owing to the boiling point constraint of IPA in which the powder has been found to undergo uniform dispersion, the experimental temperature was limited to 70°C. In a mathematical approach for estimating the probable experimental band gap reduction at sensor operating temperature, an extrapolation method has been adopted using Tauc plot method (Fig. S7).

TEM sample preparation

For TEM studies, small amounts of sample were thoroughly dispersed in isopropyl alcohol and drop casted on carbon coated copper grids (Ted Pella) of 200 mesh. Grids were allowed to undergo overnight air-drying and then mounted in the TEM machine for analysis.

FESEM sample preparation for grain size estimation

For grain size estimation, Si wafers of dimension 0.5 cmx0.5 cm were cleaned in acetone for 1 hour using a bath sonicator. The wafers were then dipped in diluted hydrofluoric acid solution in water (1:10) till the wafer floated in the acid medium, indicating that the wafer has been cleaned. Agglomeration due to Van der Waals forces is a common phenomenon during FESEM sample mounting. To avoid this, 1 M solution of CTAB (Cetrimonium bromide) was prepared in iso-propyl alcohol and the powder samples were thoroughly dispersed into it followed by drop casting on the Si wafers. The samples were then allowed to dry under UV lamp.

Surface positive charge calculation from XPS

In order to calculate the amount of surface positive charge, the core level spectra of each elemental oxidation state was deconvoluted and area under the curves were measured. The respective areas were then scaled using photo ionization cross-section values of the respective orbital and no. of scans per peak. The above values were measured with respect to composition from Rietveld refinement and a surface formula unit for each composition was determined. Then based on the respective value of oxidation states of each ionic species, total charge content per formula unit is calculated.

Table S1: Chemical composition (Al:Sn) from FESEM-EDX, TEM-EDX and XPS.

Sample	FESEM	TEM	XPS (surface specific)
$Sn_{0.947}Al_{0.144}O_{1.881}$	0.078	0.083	0.018
$Sn_{0.869}Al_{0.242}O_{1.888}$	0.146	0.108	0.044

Table S2: Area under XPS curves for aluminium doped tin oxide samples.

Sample	Relative area (in arbitrary units)
$Sn_{0.947}Al_{0.144}O_{1.881}$	Sn 3d: 36217 Al 2p: 140.55 (Al^{3+}) 22.432 (Al^{2+}) O_2^{defect}: 6095
$Sn_{0.869}Al_{0.242}O_{1.888}$	Sn 3d: 42255 Al 2p: 581.47 (Al^{3+}) 74.51 (Al^{2+}) O_2^{defect}: 5594

Table S3: Room temperature optical band gap values from UV-Vis and PL experiments.

Sample	PL	UV-Vis
$Sn_{0.933}O_2$	3.5 eV	3.49 eV
$Sn_{0.947}Al_{0.144}O_{1.881}$	3.4 eV	3.37 eV
$Sn_{0.869}Al_{0.242}O_{1.888}$	3.4 eV	3.39 eV

Table S4: Coating topography results.

Sample	S_p (Maximum height) µm	S_{mean} (Average height) µm
$Sn_{0.933}O_2$	43.99 (focus variation)	0.564 (focus variation)
$Sn_{0.947}Al_{0.144}O_{1.881}$	41.94 (focus variation)	0.589 (focus variation)
	39.24 (interferometry)	0.496 (interferometry)
$Sn_{0.869}Al_{0.242}O_{1.888}$	44.89 (focus variation)	0.654 (focus variation)
	50.76 (interferometry)	0.845 (interferometry)

Table S5: Crystallite size estimation using Scherer's formula in pure and Al doped tin oxide samples.

Sample	$Sn_{0.933}O_2$	$Sn_{0.947}Al_{0.144}O_{1.881}$	$Sn_{0.869}Al_{0.242}O_{1.888}$
Average crystallite size (nm)	9.04	7.85	5.53

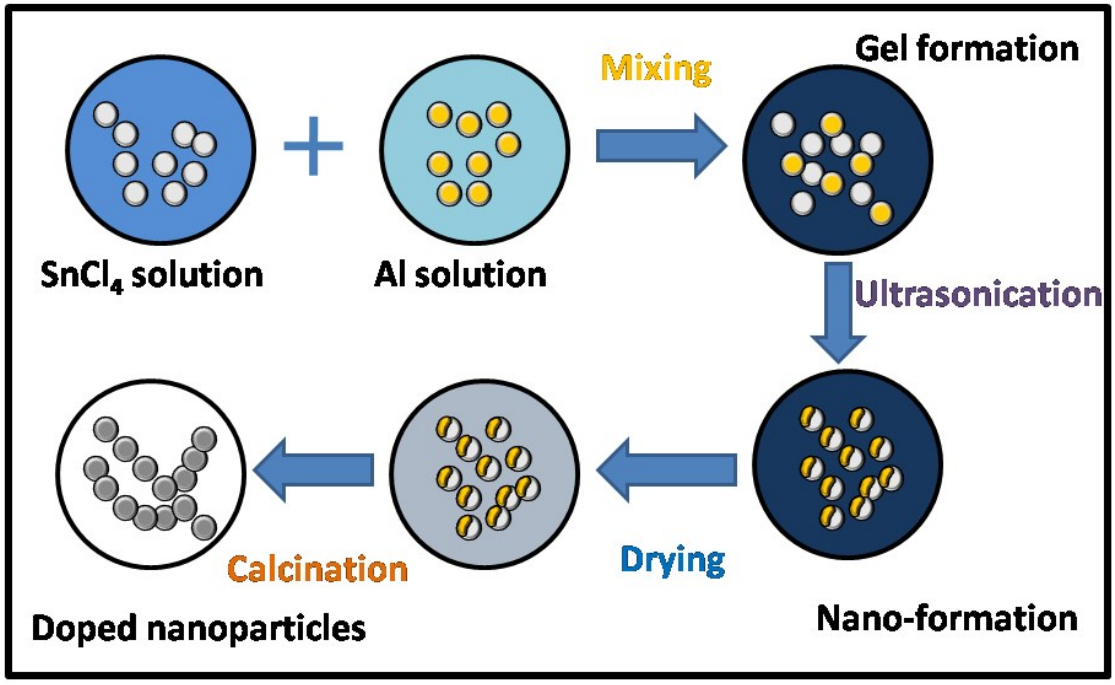

Fig. S1: Schematic of material synthesis by sol-gel method followed by ultrasonication.

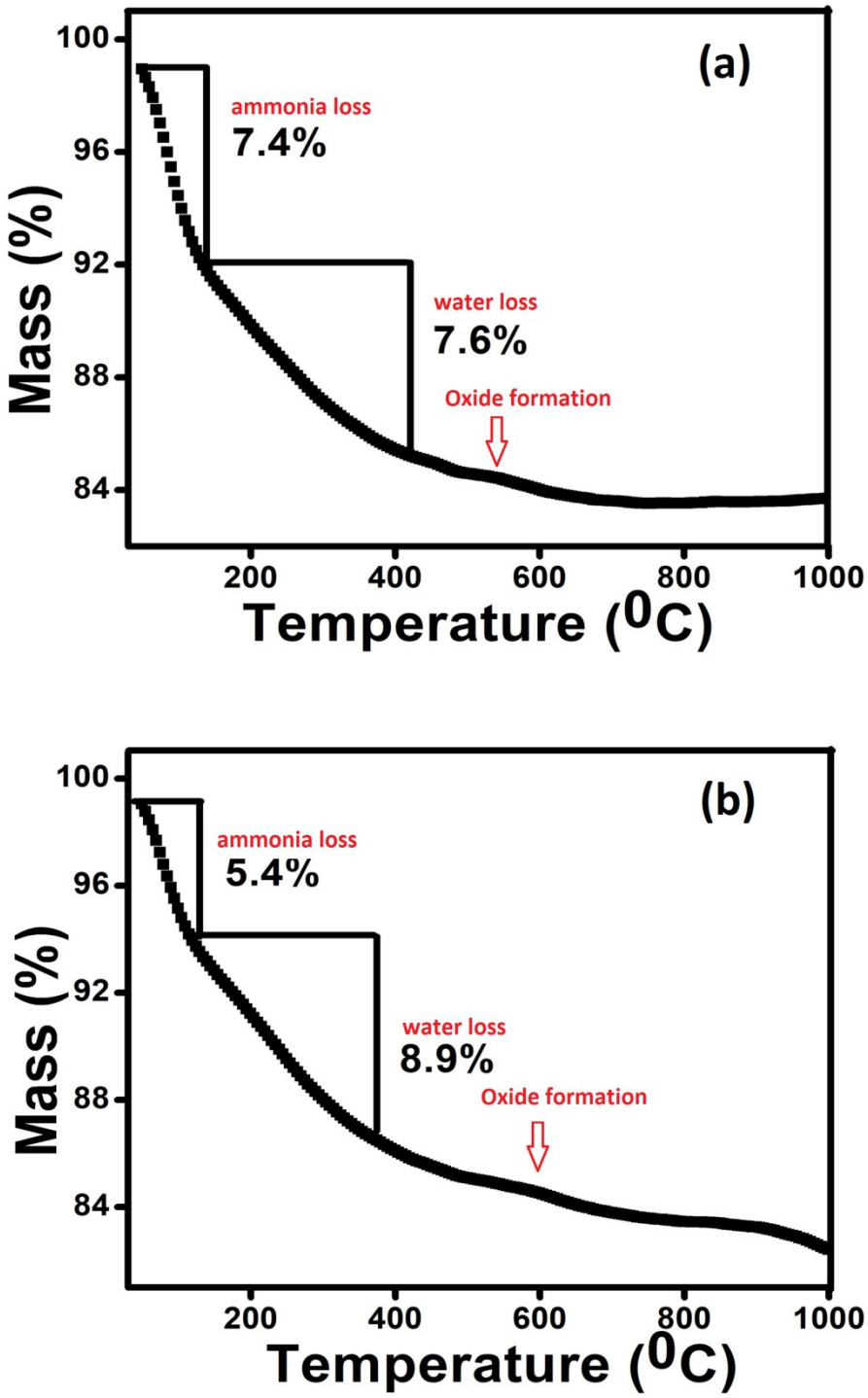

Fig. S2: TGA curves for (a) $Sn_{0.947}Al_{0.144}O_{1.881}$ (15% mass loss) and (b) $Sn_{0.869}Al_{0.242}O_{1.888}$ (14.3% mass loss) respectively, in air. The individual component loses are calculated with indication to onset of oxide formation.

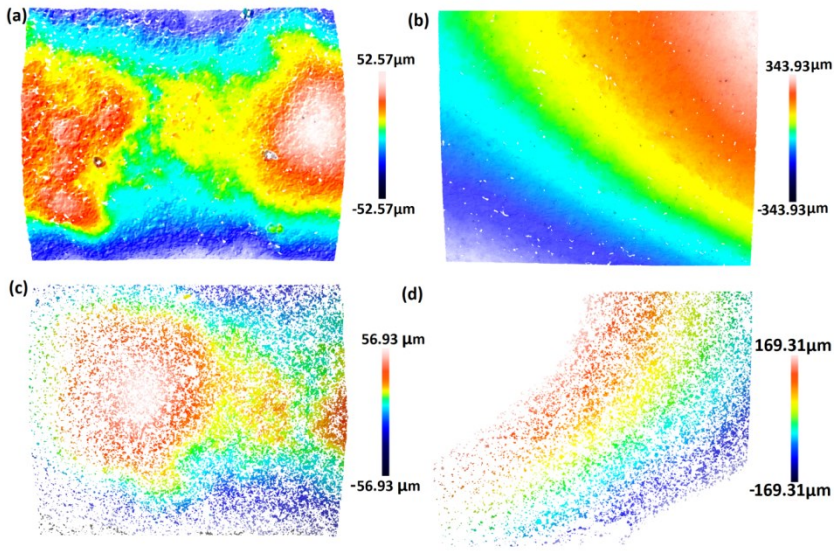

Fig. S3: Surface topography of (a) $Sn_{0.947}Al_{0.144}O_{1.881}$ and (b) $Sn_{0.869}Al_{0.242}O_{1.888}$ respectively in focus variation mode (c) $Sn_{0.947}Al_{0.144}O_{1.881}$ and (d) $Sn_{0.869}Al_{0.242}O_{1.888}$ respectively in interferometry mode. In both the modes, 20X focussing were used. Table S4 indicates at similar topographical features of all the sensor coatings.

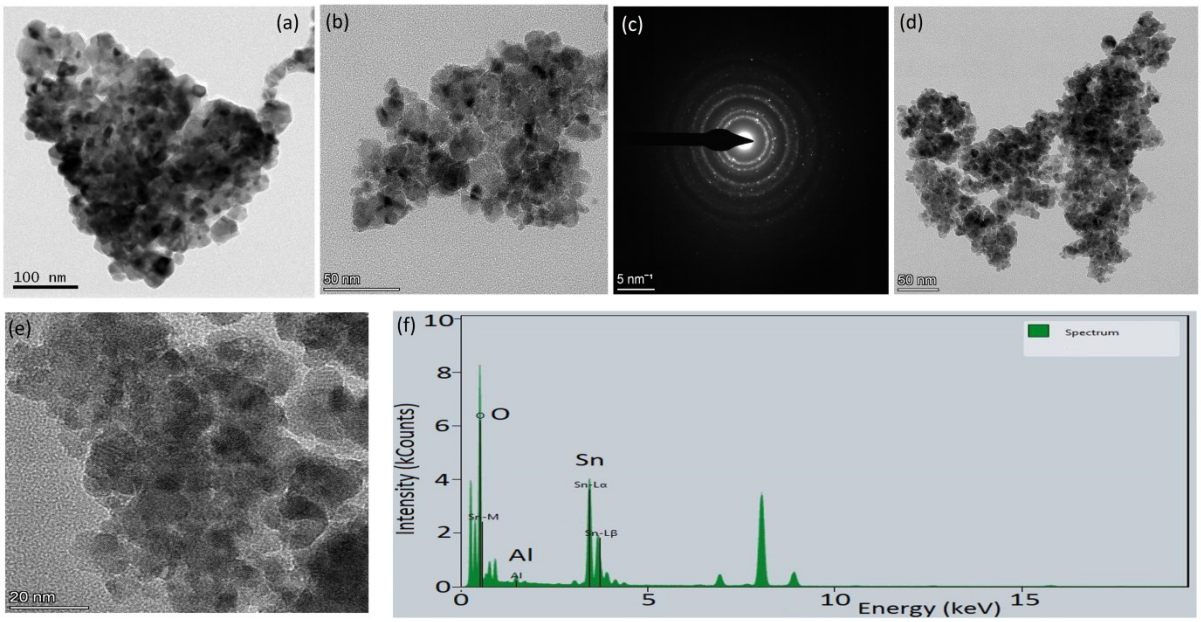

Fig. S4: (a) Bright field image of $Sn_{0.933}O_2$ (b, c) Bright field image and SAED pattern of $Sn_{0.947}Al_{0.144}O_{1.881}$ nano particles respectively (d, e) Bright field image and HRTEM micrographs of $Sn_{0.869}Al_{0.242}O_{1.888}$ respectively (f) EDX spectrum of $Sn_{0.947}Al_{0.144}O_{1.881}$.

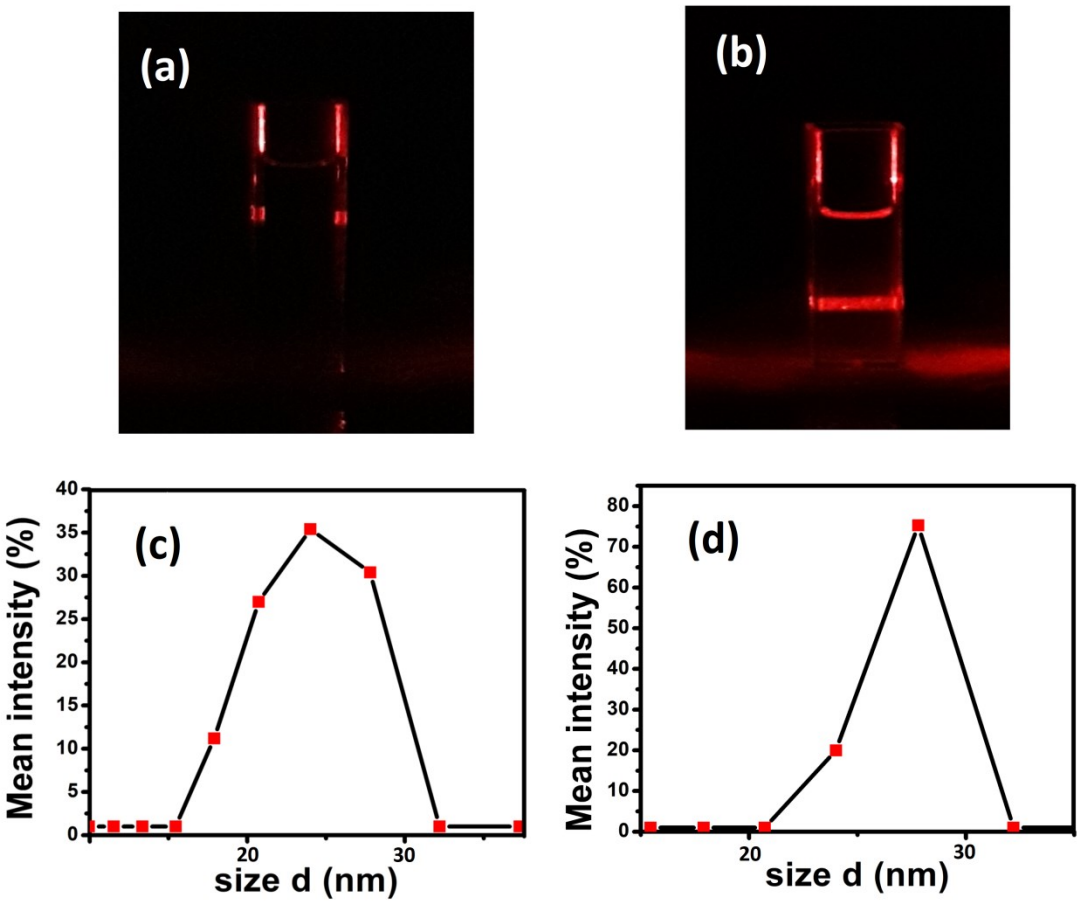

Fig. S5: DLS studies of aluminium doped tin oxide samples. (a) and (b) are figures to demonstrate uniform material dispersion in IPA medium by Tyndall effect[2] using a red laser light. (a) Pure IPA and (b) dispersion. (c) and (d) are the average particle size distribution plots for $Sn_{0.947}Al_{0.144}O_{1.881}$ and $Sn_{0.869}Al_{0.242}O_{1.888}$ respectively, where "d" is the hydrodynamic diameter in nm.

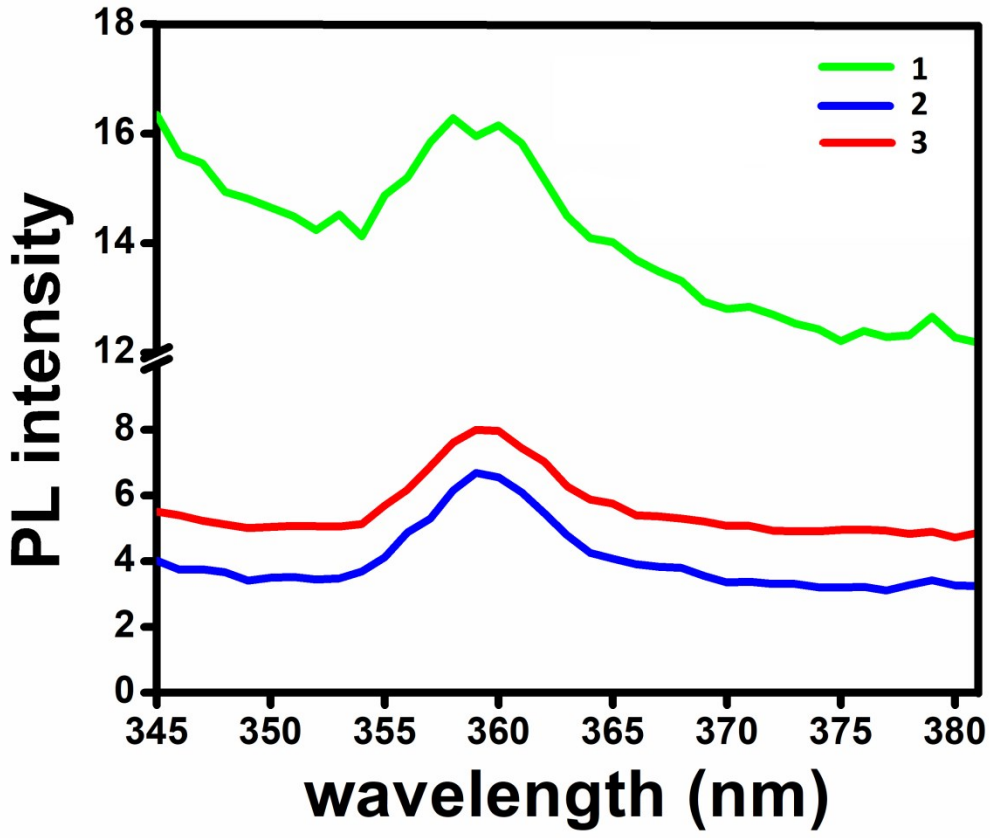

Fig. S6: Room temperature PL studies of (1) $Sn_{0.933}O_2$ (2) $Sn_{0.947}Al_{0.144}O_{1.881}$ and (3) $Sn_{0.869}Al_{0.242}O_{1.888}$ under excitation of 325 nm. No other emissions were visible within 800 nm range except those around 355-370 nm. The samples were prepared in IPA medium with concentration of 0.001 M.

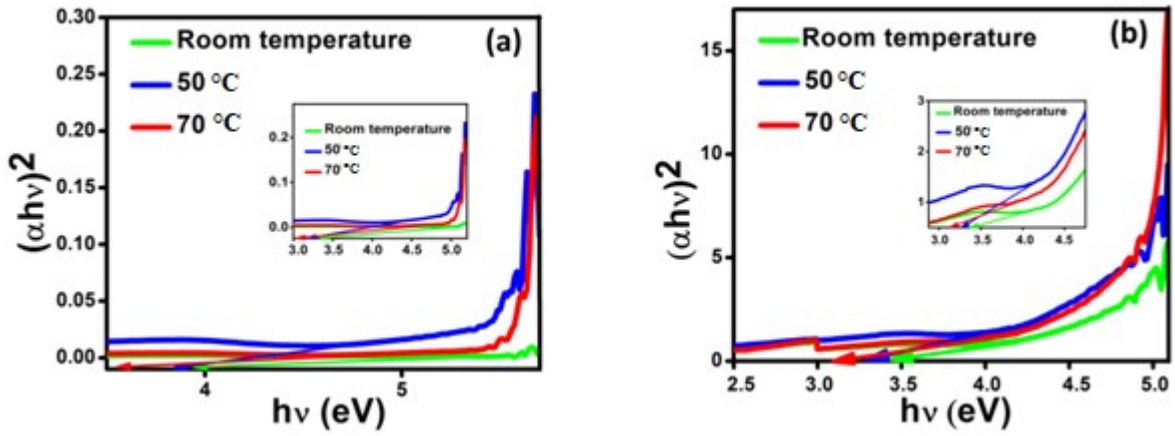

Fig. S7: Tauc plots from temperature dependent UV-Vis studies of doped tin oxide samples (a) $Sn_{0.947}Al_{0.144}O_{1.881}$and (b) $Sn_{0.869}Al_{0.242}O_{1.888}$respectively. Inset shows the intercepts in zoom. The reduction in band gap is clearly visible from shifting of intercepts towards lower energies with rise in temperature. Band gaps at room temperature were cross-checked from PL data.

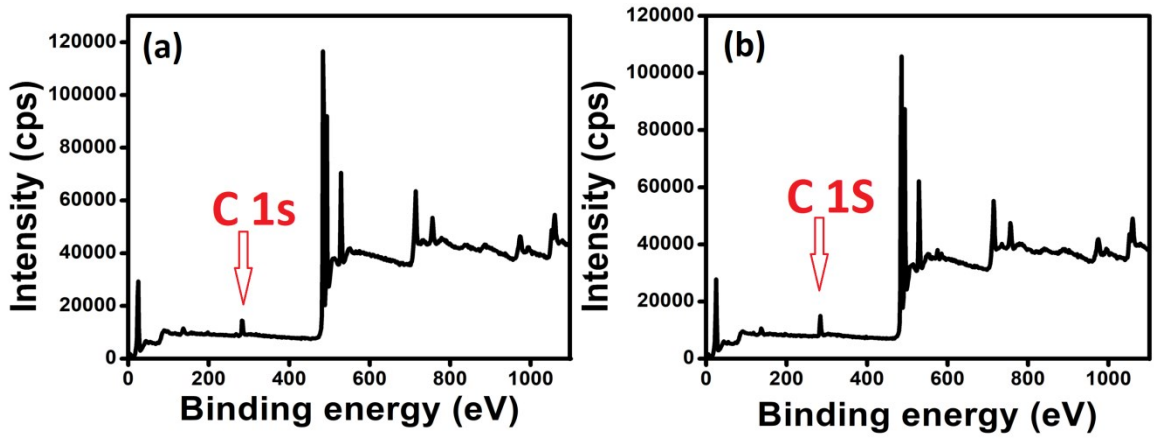

Fig. S8: XPS survey scan of (a) $Sn_{0.947}Al_{0.144}O_{1.881}$ and (b) $Sn_{0.869}Al_{0.242}O_{1.888}$ respectively. The signal corresponding to adventitious carbon is highlighted in red.

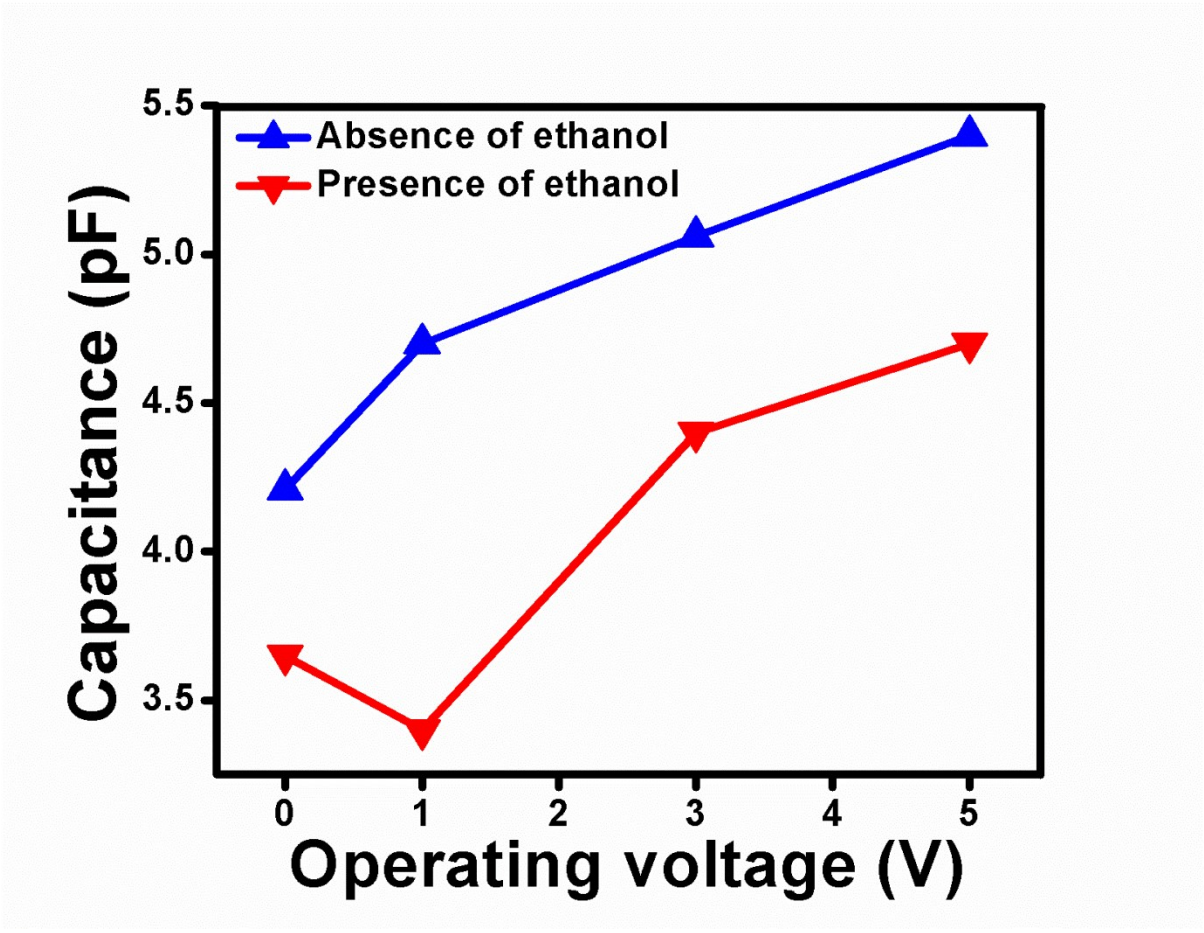

Fig. S9: Capacitance measurements in $Sn_{0.933}O_2$ at 1 kHz frequency and 1 V bias at 350°C. The change in capacitance at 350°C is negligible (as seen from the plots).

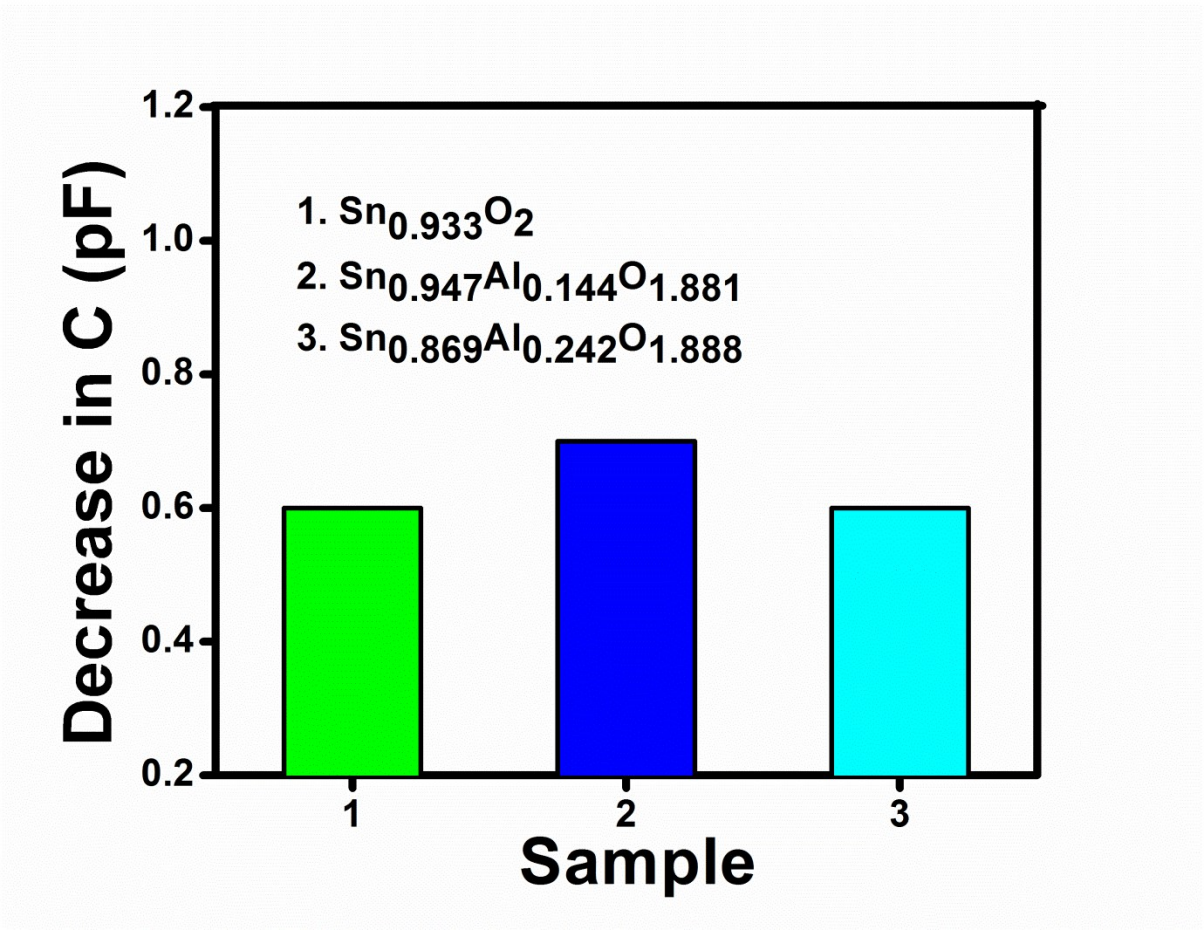

Fig. S10: Decrease in capacitance of pure and aluminium doped tin oxide samples at room temperature in presence of 5 ppm ethanol gas. The change is almost similar for all.

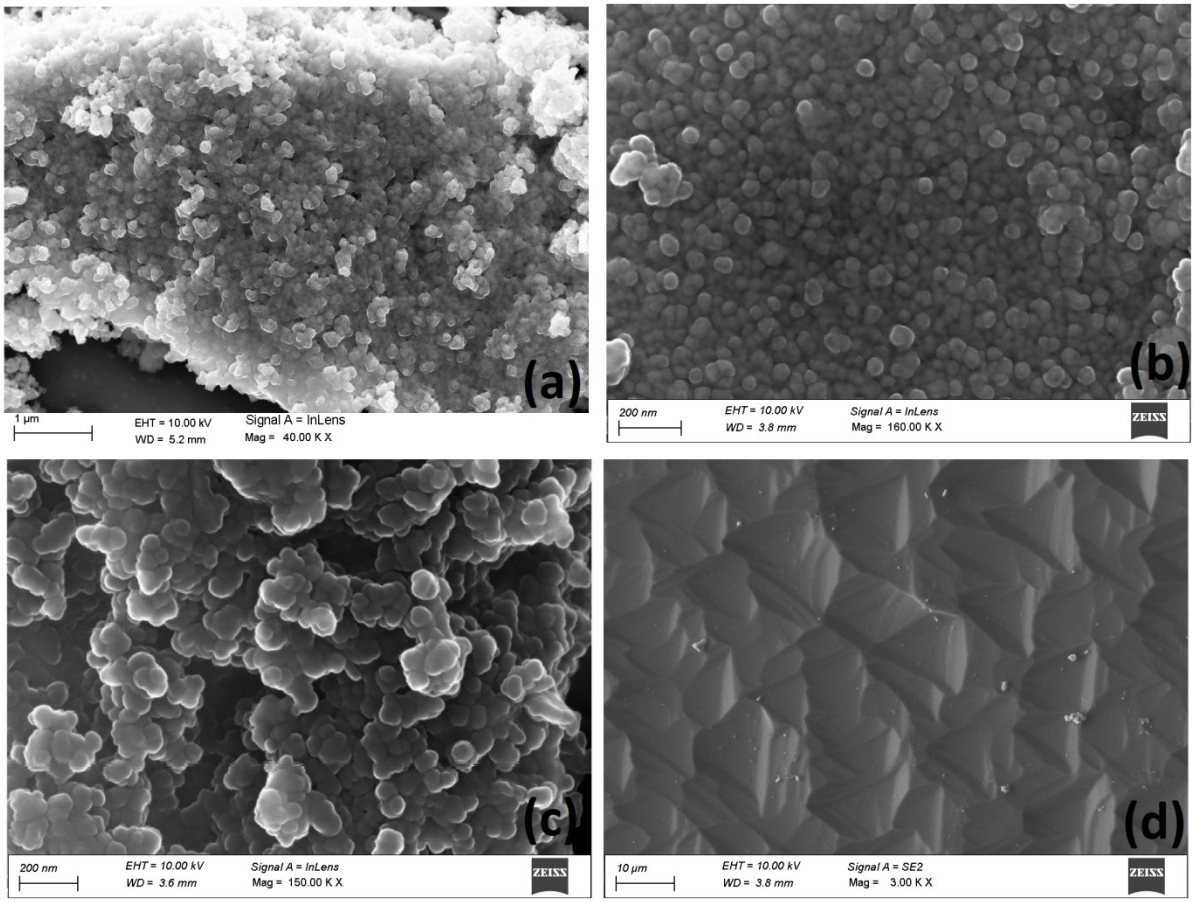

Fig S11: FESEM micrographs of (a) $Sn_{0.933}O_2$ (b) $Sn_{0.947}Al_{0.144}O_{1.881}$ and (c) $Sn_{0.869}Al_{0.242}O_{1.888}$ respectively (d) surface morphology of Si wafer. Spherical morphology and nanosized formation of tin oxide particles are visible from the images.

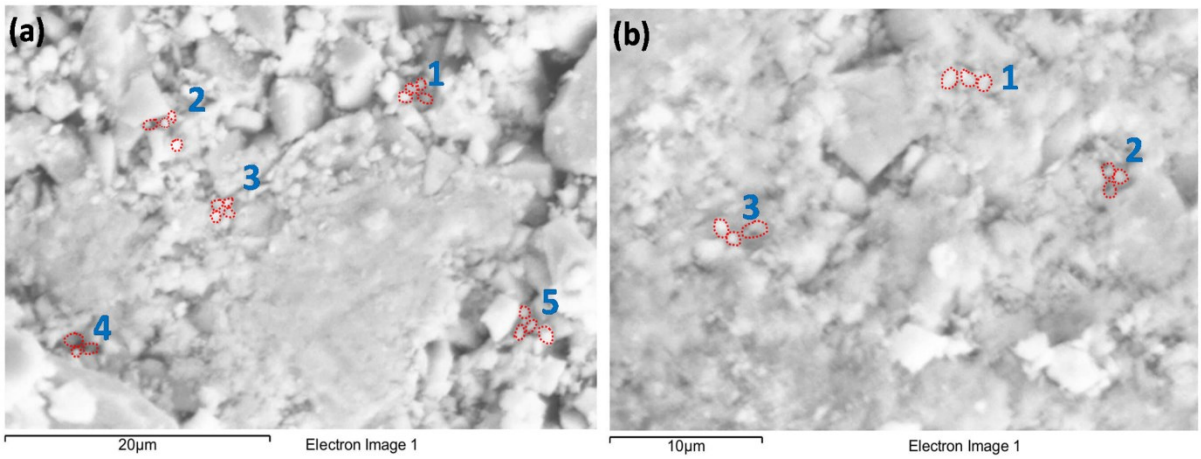

Fig. S12: (a and b) FESEM images of pelletized $Sn_{0.947}Al_{0.144}O_{1.881}$ and $Sn_{0.869}Al_{0.242}O_{1.888}$ powder samples respectively for color mapping. The pellets for this study were not sintered before experiment because that would lead to grain size enlargement by heating effects between small grains and hence checking the uniformity of doping would have been difficult.

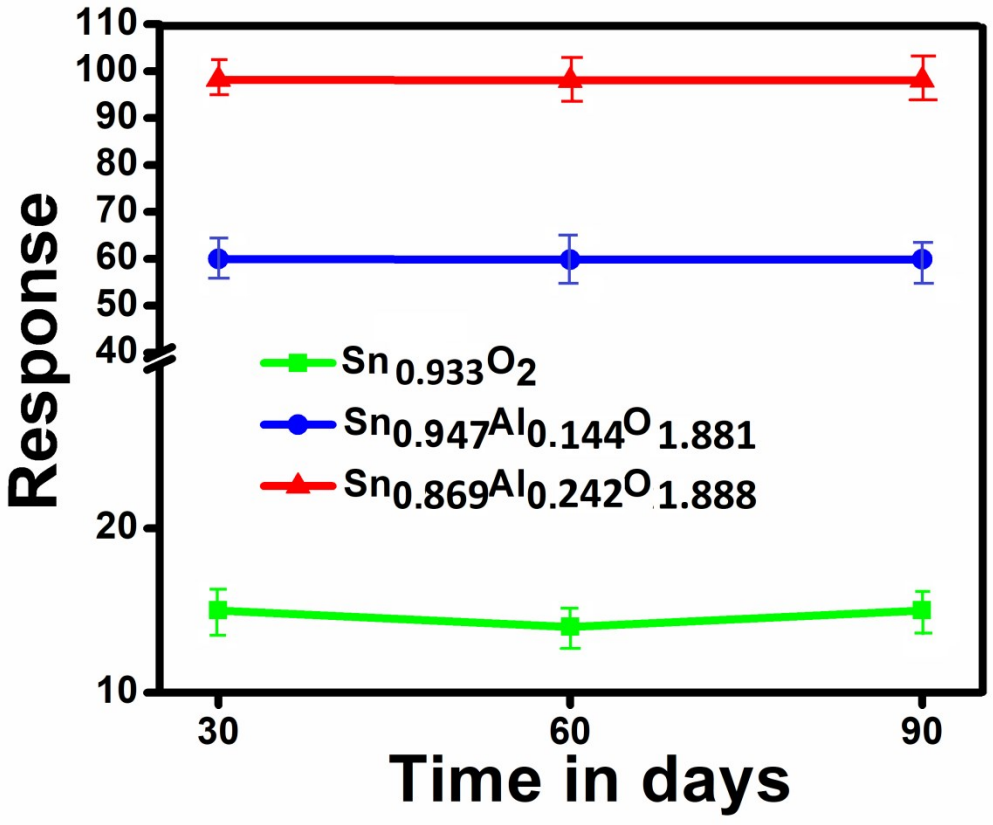

Fig. S13: Stability studies of pure and aluminium doped tin oxide sensors for 3 months with fluctuations represented by error bars. Aluminium doped sensors are highly stable even in presence of humidity.

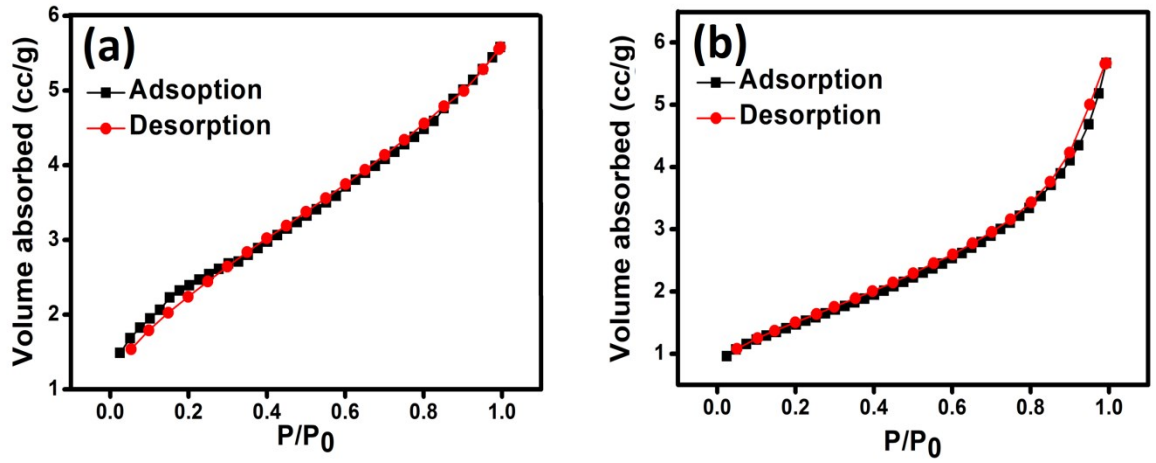

Fig. S14: Nitrogen adsorption-desorption curves for aluminium doped tin oxide nanoparticles (a) $Sn_{0.947}Al_{0.144}O_{1.881}$ and (b) $Sn_{0.869}Al_{0.242}O_{1.888}$ respectively.

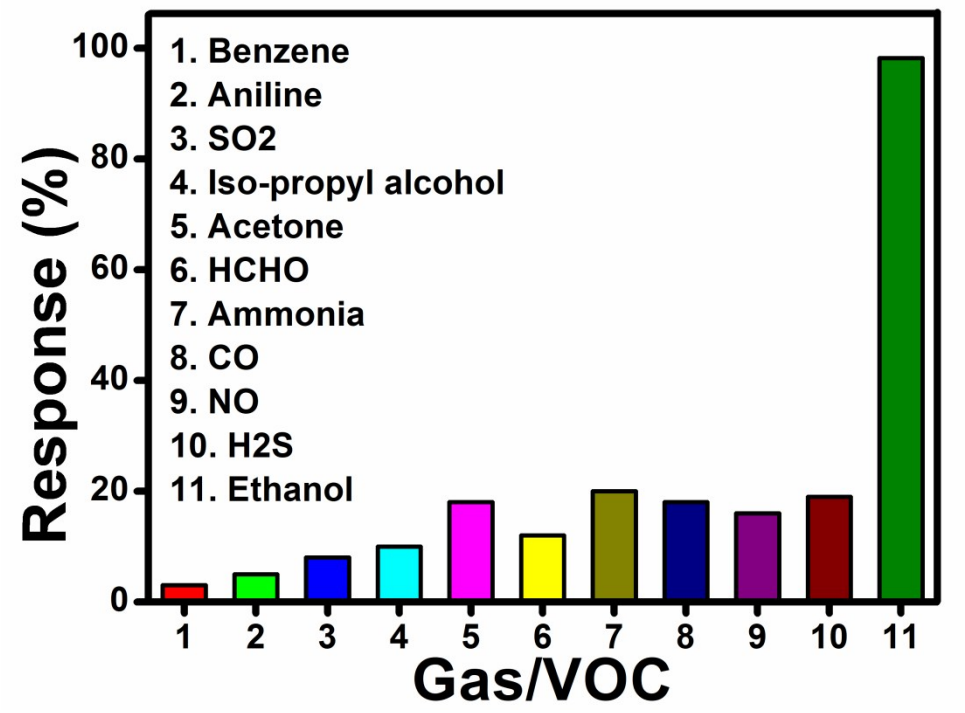

Fig. S15: Cross sensitivity plot for $Sn_{0.869}Al_{0.242}O_{1.888}$ under identical conditions of 5 ppm ethanol sensing.

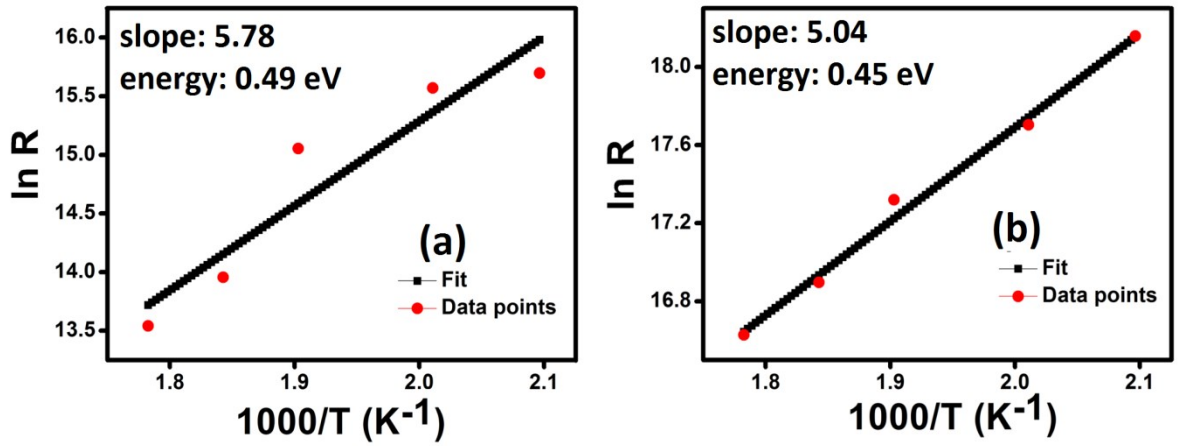

Fig. S16: ln R vs. 1000/T curves for (a) $Sn_{0.947}Al_{0.144}O_{1.881}$ and (b) $Sn_{0.869}Al_{0.242}O_{1.888}$ respectively.[3] Inter-granular activation energies are similar for both samples.

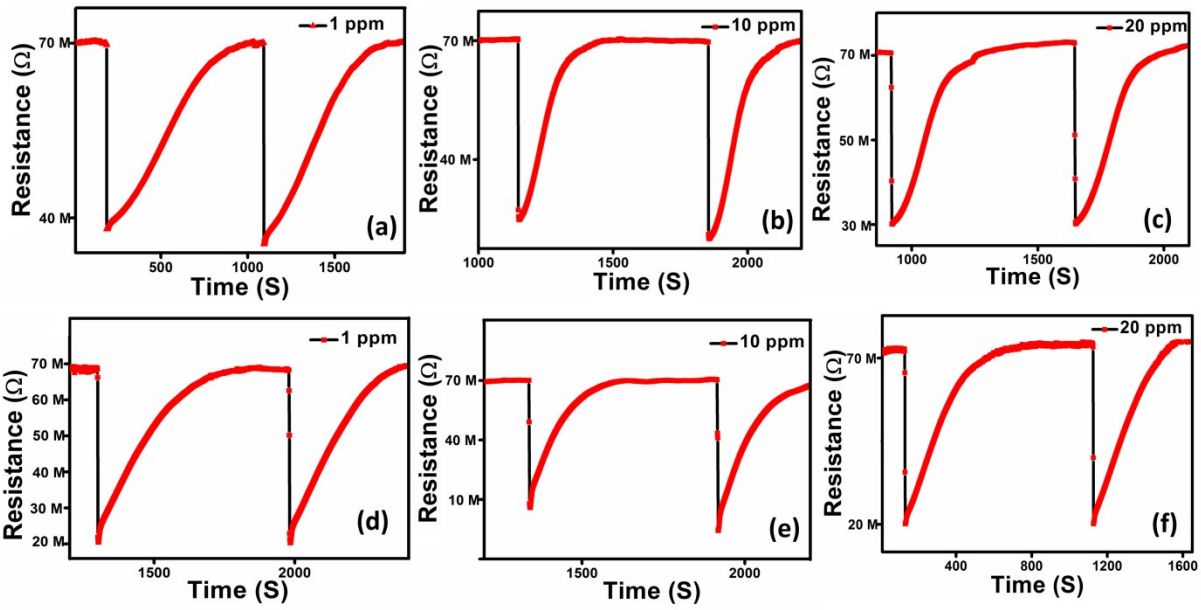

Fig S17: Dynamic sensing responses to different ppm of ethanol vapour (a, b, c) by $Sn_{0.947}Al_{0.144}O_{1.881}$ and (d, e, f) $Sn_{0.869}Al_{0.242}O_{1.888}$ samples respectively.

References

[1] Zhang, J.; Gao, L. Synthesis and characterization of nanocrystalline tin oxide by sol–gel method Journal of Solid State Chemistry 2004, 177, 1425–1430.

[2] Kraemer, E. O.; Dexter, S. T. The light-scattering capacity (Tyndall effect) and colloidal behaviour of Gelatin sols and gels J. Phys. Chem. 1927, 31, 5, 764–782.

[3] Gönüllü, Y.; Haidry, A. A.; Saruhan, B. Nanotubular Cr-doped TiO_2 for use as high-temperature NO_2 gas sensor Sensors and Actuators B 2015, 217, 78–87.